Multipath distributed acoustic sensing system based on phase-sensitive optical time-domain reflectometry with frequency division multiplexing technique

Kun Zhu[a], Bin Zhou[b], Huan Wu[a,*], Chao Shang[c], Linyue Lu[d], Muhammad Adeel[a], Yaxi Yan[a], Zhiyong Zhao[a], Hwa-Yaw Tam[d], and Chao Lu[a]

[a] *Photonics Research Centre, Department of Electronic and Information Engineering, The Hong Kong Polytechnic University, Hong Kong, PR China*
[b] *South China Academy of Advanced Optoelectronics, South China Normal University, Guangzhou 510631, PR China*
[c] *Key Laboratory of Luminescence and Optical Information, Ministry of Education, Institute of Optical Information, School of Science, Beijing Jiaotong University, Beijing, PR China*
[d] *Photonics Research Centre, Department of Electrical Engineering, The Hong Kong Polytechnic University, Hong Kong, PR China*

* Corresponding author.
E-mail addresses: kun.zhu@polyu.edu.hk (K. Zhu), zhoubin_mail@163.com (B. Zhou), hkpolyu.wu@polyu.edu.hk (H. Wu), cshang@bjtu.edu.cn (C. Shang), lulinyue@gmail.com (L. Lu), m.adeel@connect.polyu.hk (M. Adeel), ya.xi.yan@connect.polyu.hk (Y. Yan), zhiyong.zhao@polyu.edu.hk (Z. Zhao), hwa-yaw.tam@polyu.edu.hk (H.-Y. Tam), enluchao@polyu.edu.hk (C. Lu)

Abstract

We propose a multipath distributed acoustic sensing (MP-DAS) system based on phase-sensitive optical time-domain reflectometry (Φ-OTDR) and frequency division multiplexing (FDM) technique. With FDM introduced to Φ-OTDR, simultaneously monitoring of multipath vibration is realised with flexible functionality. In the proposed MP-DAS system, the parameters of each path can be adjusted individually according to the path's specific monitoring requirement. A dual path Φ-OTDR system with 1 km and 22 km measurement distance is demonstrated in the experiment. Through heterodyne detection and FDM technique, both amplitude and phase information are obtained for event locating and vibration sensing in each of the two paths, with a spatial resolution of 5 m and 10 m respectively. With changing optical power and pulse width of one path, its influence on the other path is discussed and analysed. This proposed MP-DSA system based on FDM technique provides an efficient and cost-effective way for upgrading a conventional single DAS into an integrated DAS network, which shows great potential in many applications such as modern city civil structure monitoring with different demands.

Keywords: Distributed optical fibre sensor, distributed acoustic sensing, phase-sensitive OTDR, frequency division multiplexing, coherent detection.

1. Introduction

Distributed optical fibre sensing (DOFS) systems have attracted great interests recently and been investigated extensively in both academic and industrial fields due to its inherent advantages of light weight, high sensitivity, compactness, immunity to electromagnetic interference (EMI), passive remote sensing, *etc*. [1-10]. A wide range of sensing parameters, such as strain, temperature and acoustic disturbance, can be measured by detecting and

analysing different types of backscattering of light in a sensing fibre, *i.e.*, Rayleigh backscattering, Brillouin backscattering, and Raman backscattering [1]. As one of the most attractive DOFS technologies for dynamic strain sensing or fast-changing parameter monitoring, phase-sensitive optical time-domain reflectometry (Φ-OTDR) utilizes the information of coherent Rayleigh backscattering in time domain, which has been seen as the optimal implementation for the so-called distributed acoustic sensing (DAS) or distributed vibration sensing (DVS) systems [11-23]. The DAS systems based on Φ-OTDR have shown great potential in a variety of engineering applications including border security, civil structural health monitoring, gas or oil pipeline integrity monitoring and threat detection, geophysical applications, railway system monitoring, *etc*. [2-10]. Therefore, plenty of work has been done by researchers and engineers to investigate the fundamental theory and propose various implementations of Φ-OTDR [12-15]. To exactly extract the phase information from the backscattering signal of Φ-OTDR, various schemes have been proposed, such as a basic Φ-OTDR setup using dual pulses with certain frequency difference [16], methods based on direct detection merging different types of interferometers [17-19], a coherent Φ-OTDR scheme based on heterodyne detection [20-22], and a coherent Φ-OTDR scheme based on homodyne detection with IQ demodulation [23]. Meanwhile, efforts have been made to improve the sensing performance of the Φ-OTDR with longer sensing distance and higher spatial resolution in one sensing fibre.

In the metropolitan area of a modern city, *e.g.*, Hong Kong, various civil structures exist jointly with urban metro system and different types of pipelines. As an example, shown in Fig. 1, for a full-view monitoring in this metropolitan scenario, proper DAS systems should be installed to all the urban large-scale construction, the river/sea-spanning bridge and the metro tunnel/viaduct, but with different requirements on the sensing distance, spatial resolution, frequency response, *etc*. It is complicated and not cost-effective to build a single Φ-OTDR for each of them. Efficiently merging several Φ-OTDR systems into one would offer the DAS extra flexibility and versatility. There is a demand to upgrade a single DAS system to an integrated DAS network.
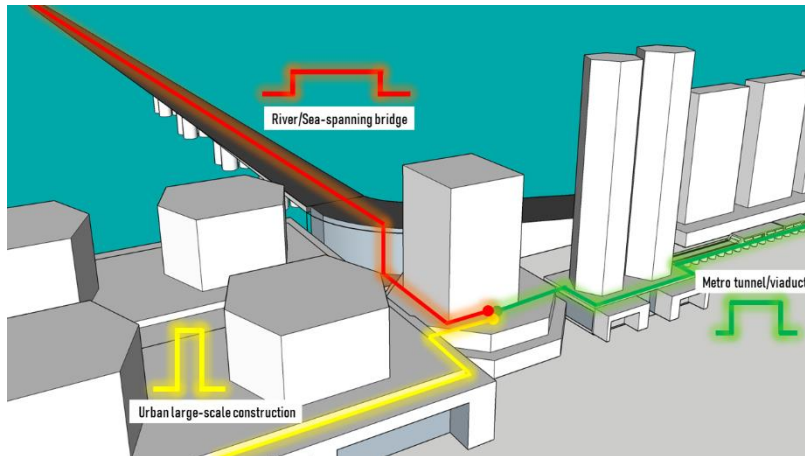

Fig. 1. DAS scenario in the metropolitan area of a modern city

In this paper, we propose a multipath DAS (MP-DAS) system based on Φ-OTDR and frequency division multiplexing (FDM) technique. With the technique of frequency division multiplexing and demultiplexing, Φ-OTDR with different sensing parameters can be implemented onto each individual path of sensing fibre, and the phase information from every path due to fibre disturbance can be detected and recovered together with sharing one optical source and signal receiving end. More than one distributed optical paths are monitored simultaneously in this proposed scheme, so that a flexible DAS network is built. It is worth

noting that in such an MP-DAS system, the parameters of each path can be adjusted individually according to the path's specific monitoring requirement, and the overall cost is reduced since only one optical source and receiver are used. In the proof-to-concept experiment, a dual path Φ-OTDR system with 1 km and 22 km distance is demonstrated. The modulated light pulses with different pulse width and repetition rate are launched into the two sensing fibres respectively, which gives different required spatial resolutions to the two paths. The location and vibration information of both the paths is successfully extracted. By changing the optical power and pulse width of one path, we for the first time analyse the influence on the signal-to-noise ratio (SNR) to the other path in detail for the MP-DAS based on FDM technique, and discuss the possible way to increase one path's SNR without affecting the others. The experimental results show that even with other paths' interference, we still locate the event and recover the vibration signal with neglectable SNR deterioration, which shows good performance of our proposed DAS network for multipath monitoring.

2. Principle

FDM is a technique that has been widely employed in a variety of communication systems to massively increase data communication capacity [24]. Recently FDM technique has been introduced to the Φ-OTDR systems in order to increase the signal-to-noise ratio (SNR) [25,26], to enlarge the frequency response range of the measured vibration [27-30], and to improve the spatial resolution with the enhanced optical pulse compression technique based on linear frequency modulation (LFP) [31,32]. In our proposed scheme, FDM technique is utilized to implement Φ-OTDR to multiple fibre paths based on a single optical transmitter and receiver, but with different measurement parameters, as shown in Fig. 2. Besides FDM technique, multi-wavelength optical lasers can also be used to achieve the same functionality. However, considering the narrow linewidth requirement of the laser for Φ-OTDR, it is more challenging and not economy to employ a stable multi-wavelength narrow-linewidth laser other than the FDM technique.
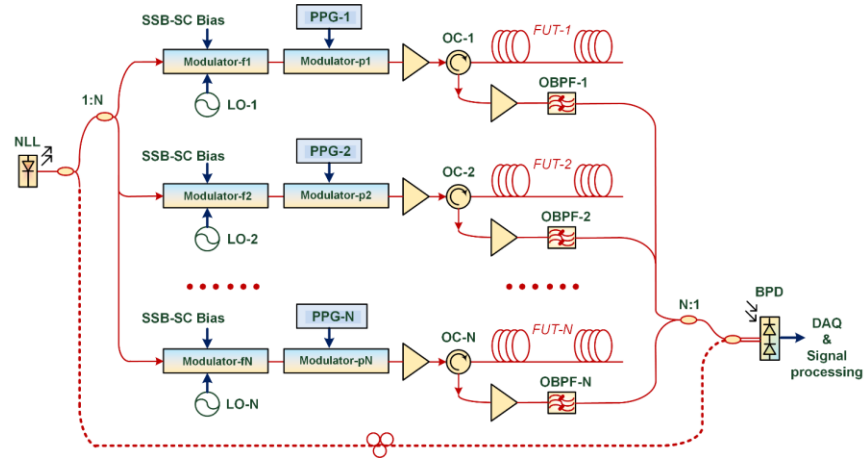

Fig. 2. General schematic of the proposed MP-DAS system (NLL: narrow-linewidth laser; SSB-SC: single-sideband suppressed-carrier modulation; LO: local oscillator; PPG: pulse pattern generator; OC: optical circulator; OBPF: optical bandpass filter; FUT: fibre under test; BPD: balanced photodetector.)

Fig. 2 shows a general schematic of the proposed multipath Φ-OTDR system. In this system, the lightwave from a narrow-linewidth laser is divided into $N+1$ fractions, in which N portions are used as the probe lights and the last one is used as the local oscillator (LO). The electrical field can be written as

$$E_{in}(t) = E_0 \exp\left[j(2\pi f_0 t + \phi_0)\right]$$
$$= \sum_{i=1}^{N} E_i \exp\left[j(2\pi f_0 t + \phi_i)\right] + E_{LO} \exp\left[j(2\pi f_0 t + \phi_{LO})\right] \tag{1}$$

where E_i is the scalar amplitude of the i-th probe lightwave, E_{LO} is the scalar amplitude of the LO lightwave, f_0 is the optical frequency, and ϕ stands for the initial phase term of each light path. For each of the probe branches, the lightwave is first modulated by a frequency modulator (*e.g.*, undergoing single-sideband suppressed-carrier modulation (SSB-SC)) to get a certain frequency shift Δf_i for the FDM, and then modulated by a high extinction ratio modulator driven by a pulse pattern generator (PPG) to become a probe light pulse, which can be described as

$$E_{i-pulse}(t) = E_i P_i(t) \exp\left[j(2\pi(f_0 + \Delta f_i)t + \phi_i)\right] \tag{2}$$

where $P_i(t)$ is the waveform of the i-th probe pulse. In this case, the frequency shift Δf_i for each path can be adjusted individually and flexibly, and the extinction ratio of the light pulse is determined by the second modulator in this branch according to its specific demands. Assuming that the coherence length of the laser is much larger than twice of the fibre under test (FUT), the coherent Rayleigh backscattering (RBS) lightwave can be described as

$$E_{RBS-i}(t) = R_i(t) \exp\left[j(2\pi(f_0 + \Delta f_i)t + \varphi_i(t) + \phi_i)\right] \tag{3}$$

where $R_i(t)$ and $\varphi_i(t)$ are the RBS amplitude and phase coefficients of the i-th probe pulse respectively. Finally, all the RBS and the LO lightwaves are mixed together in an optical coupler and then detected by a balanced photodetector (BPD). The detected photocurrent is proportional to the total optical power, and can be expressed as

$$I(t) \propto E_{LO}^2 + \sum_{i=1}^{N} R_i^2(t) + 2E_{LO}\sum_{i=1}^{N} R_i(t)\cos\left(2\pi\Delta f_i t + \varphi_i(t) + \phi_i - \phi_{LO}\right)$$
$$+ 2\sum_{i=1}^{N-1}\sum_{j=i+1}^{N} R_i(t)R_j(t)\cos\left[2\pi\left(\Delta f_i - \Delta f_j\right)t + \varphi_i(t) - \varphi_j(t) + \phi_i - \phi_j\right] \tag{4}$$

It should be mentioned that there are restrictions on the selection of frequency shifts of all the paths. The largest frequency shift should be within the bandwidth of the BPD, and also out of the frequency range of Brillouin scattering (*i.e.*, around 10-11 GHz for Standard single mode fibre, which is too high for our application.) to avoid additional nonlinear noise. The frequency spacings of the two adjacent channels (*i.e.*, $\Delta f_{i+1} - \Delta f_i$) should be large enough to suppress the crosstalk. But too large frequency spacings will limit the total path number with a certain BPD bandwidth B. Assuming that all the frequency spacings are same, and simply equal to the first path frequency shift Δf_1, the total path number N will be limited by $B/\Delta f_1$, which shows the multiplexing ability of the system. This ability of multiplexing can be strengthened when a BPD with larger bandwidth is used, but this will increase the system cost when the bandwidth B goes extremely high.

By carefully selecting Δf_i and the following electrical or digital bandpass filters, all the DC components and the second AC component in Eq. (4) can be filtered out, so that only the first AC component with certain frequency remains. In this way, the output signal is demultiplexed, and the sensing signal from each branch with selected frequency Δf_i is mixed by $\cos(2\pi\Delta f_i)$ and $\cos(2\pi\Delta f_i + \pi/2)$ respectively, then filtered by a proper low pass filter (LPF) digitally. The output is shown as below,

$$\begin{cases} I_{AC-i} = E_{LO}R_i(t)\cos\left(\varphi_i(t) + \phi_i - \phi_{LO}\right) \\ Q_{AC-i} = E_{LO}R_i(t)\sin\left(\varphi_i(t) + \phi_i - \phi_{LO}\right) \end{cases} \tag{5}$$

Thus, the amplitude and phase coefficients of the RBS lightwave from the i-th branch can be extracted as

$$\begin{cases} R_i(t) \propto \sqrt{I_{AC-i}^2 + Q_{AC-i}^2} \\ \varphi_i(t) = \arctan\left(Q_{AC-i}/I_{AC-i}\right) - \left(\phi_i - \phi_{LO}\right) \end{cases} \tag{6}$$

Finally, both the amplitude and phase information from all the sensing branches can be demultiplexed and demodulated. The amplitude differentiation of two traces with certain

interval can be used for fast event locating. The phase change of a certain length of fibre can also be obtained by differentiating the phase between the corresponding distance interval. Additional phase unwrapping algorithm is used to extend the demodulated phase range from -$\pi/2$ to $+\pi/2$ to $-\infty$ to $+\infty$. Based on this, the demodulated phase change can be seen in linear with the induced strain by fibre vibration.

3. Experiment and discussion

As a poof-to-concept demonstration, we build a dual path Φ-OTDR system. Fig. 3 shows the experimental setup. A narrow-linewidth laser (Connet CoSF-SC-1550-M) with 5 kHz linewidth is employed as the coherent optical source. Its output power is 3 dBm with the central wavelength at 1550.1 nm. The lightwave is first split by a 95:5 coupler into two parts. 5% lightwave is used as the LO light for the heterodyne detection. The rest 95% lightwave is then split again by a 50:50 coupler into two branches as the probe lights. It is worth noting that for a practical application, the coupling ratio of the fibre couplers can be selected specifically according to the power requirement of different FUT paths. In the upper branch, the probe light is modulated by an acousto-optic modulator (AOM) with a frequency shift of 100 MHz, which fulfils the functions of frequency shift and pulse modulation simultaneously. An electrical pulse from an arbitrary waveform generator (AWG, BK Precision 4065) is amplified by the AOM driver, then drives the AOM to get the required probe light pulse, whose width is 100 ns with a repetition rate of 2 kHz. After amplification by an erbium-doped fibre amplifier (EDFA, Amonics AEDFA-18-M-FA) and filtering by a 100 GHz optical bandpass filter (OBPF), the probe light pulse is launched into the first FUT with 22 km length through an optical circulator. Along the FUT, a length of 10 m bare standard single mode fibre is coiled around a cylindrical piezoelectric transducer (PZT) at the far end as the vibration generator. The RBS signal from the third port of the optical circulator is then amplified by another EDFA (Amonics AEDFA-PA-35-B-FA) and filtered by another 100 GHz OBPF to get the required power lever and SNR for coherent detection. We should mention that the peak power of the amplified optical pulse should be controlled, since too large power will generate Brillouin signal, and this will introduce additional nonlinear noise. For the lower branch, the setup is similar but with different sensing parameters, *i.e.,* the frequency shift of the AOM is 80 MHz; the probe light pulse is with a width of 50 ns and a repetition rate of 50 kHz. The FUT is a 1 km standard single mode fibre with a length of 5 m spirally adhered to the surface of a sounder at the end. Finally, the RBS traces from the two sensing paths are combined and mixed with the LO lightwave through two fibre couplers, and the beating signal is detected by a BPD (Thorlabs PDB465C) with a bandwidth of 200 MHz. The electrical signal from the BPD is then sampled by an oscilloscope (Picoscope 4425) with a sample rate of 625 MS/s. All the digital signal processing work is done with MATLAB on a personal computer. Compared with the general system structure shown in Fig. 2, the experimental setup in Fig. 3 shows a simplified implementation. Only one AOM is used in each branch in this simpler setup. But in this case, the frequency shifts are fixed and determined by the characteristics of the AOMs. The extinction ratios and frequency shifts of the AOMs should be chosen and optimized carefully, so that the crosstalk can be eased and the paths can be monitored as many as possible.
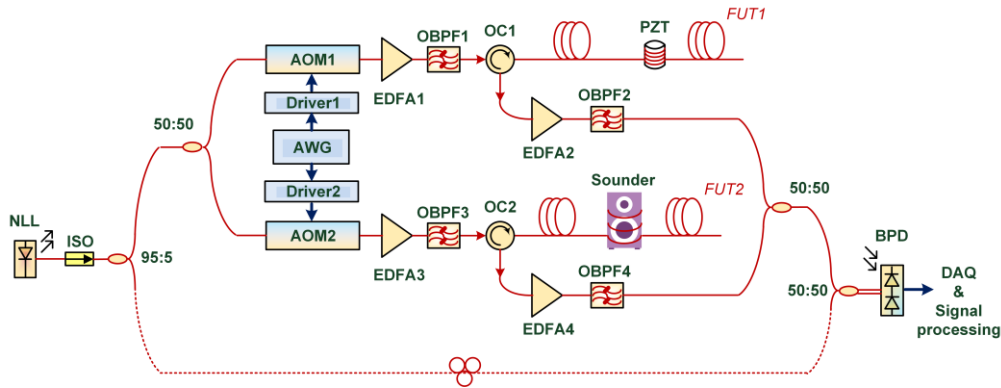
Fig. 3. The experimental setup of the dual path Φ-OTDR system (NLL: narrow-linewidth laser; ISO: isolator; AWG: arbitrary waveform generator; AOM: acousto-optic modulator; EDFA: erbium-doped fibre amplifier; OBPF: optical bandpass filter; OC: optical circulator; PZT: piezoelectric transducer; FUT: fibre under test; BPD: balanced photodetector.)

Fig. 4 shows th detected RBS traces of the dual path Φ-OTDR system from the oscilloscope. It is obvious that the speckle pattern shown in Fig. 4 is a mixed product as the superimposition of the two conventional Φ-OTDR traces from both upper and lower sensing branches. There are in total two cycles for the 500 μs trace and fifty cycles for the 20 μs trace in 1 ms time window as shown Fig. 4, corresponding to their repetition rates of 2 kHz and 50 kHz for the two branches with different sensing lengths respectively. These two mixed RBS signals in the time domain will be demultiplexed and demodulated through digital filtering and frequency mixing.
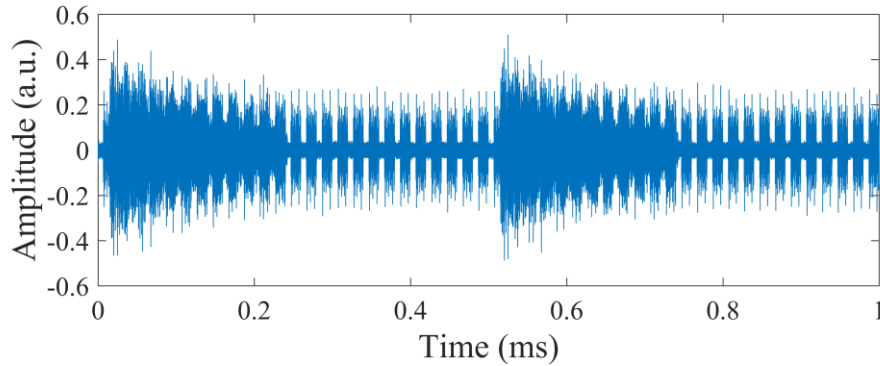

Fig. 4. The detected Rayleigh backscattering traces of the dual path Φ-OTDR system

The sampled signal is first demultiplexed by two digital 10 MHz bandpass filters centred at 100 MHz and 80 MHz respectively, then mixed by the sine and cosine signals at the corresponding frequencies, followed by the low pass filters to suppress the high frequency AC components. The amplitude information is calculated according to Eq. (6) for fast disturbance locating. By differentiating two amplitude traces with certain intervals, *e.g.*, subtracting all the amplitude traces from the first one, the disturbance locations of both the sensing paths can be observed, as shown in Fig. 5. Fig. 5(a) shows 50 superimposed differential amplitude traces for the 22 km sensing path, in which a visible peak can be observed at the location of the external vibration caused by the 10 m PZT. As the probe pulse width for this branch is 100 ns, a theoretical spatial resolution of 10 m is achieved. As for the 1 km sensing path, Fig. 5(b) shows 50 superimposed differential amplitude traces with a spatial resolution of 5 m. A peak is found at the location of the sounder due to the sine voice broadcasted from it. We see that the

disturbance locations for both the branches are indicated successfully in our dual path Φ-OTDR system with FDM technique.

As a comparison, separate measurements have been carried out for both the branches individually. In the separate measurement, for the individual upper or lower branch depicted in Fig. 3, the two EDFAs in the other branch are turned off, and all the parameter settings keep unchanged. In this case, there is no FDM, and the standard Φ-OTDR with heterodyne detection is carried out for the two sensing paths individually. Fig. 6 shows their results as compared with the corresponding outcomes in Fig. 5. For the upper branch with 22 km sensing path, the SNR decreases from 15.1 dB to 13.7 dB due to the FDM interference. For the lower branch with 1 km sensing path, the SNR decreases from 22.1 dB to 18.8 dB. The SNR is deteriorated due to the crosstalk between the two RBS signals of different frequencies. In this work, rectangular pulses are used as the sensing probe. The sidelobes of these rectangular pulses actually contribute to the crosstalk. To ease this issue, Gaussian-like pulses can also be used [33-35].
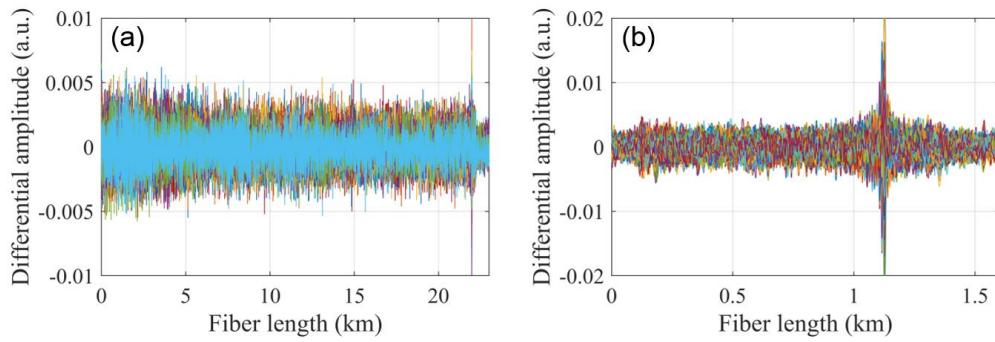

Fig. 5. The detected disturbance locations for the two sensing paths with FDM and joint demodulation, (a) for the 22 km branch, (b) for the 1 km branch.
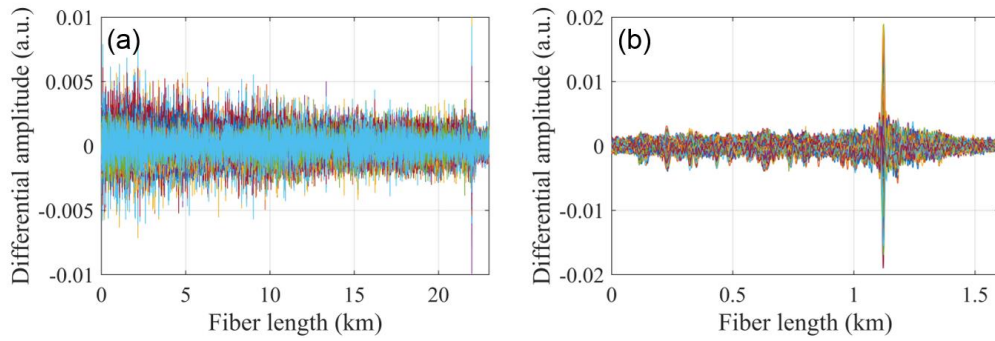

Fig. 6. The detected disturbance locations for the two sensing paths with separate measurement, (a) for the 22 km branch, (b) for the 1 km branch.

The phase information is also successfully extracted. Through additional unwrapping algorithm, the actual vibration signals can be retrieved at the vibration locations. In the experiment, a sinusoidal signal with 5 V magnitude and 100 Hz frequency is used to drive the 10 m PZT in the 22 km sensing path. For the 1 km sensing path, a 1 kHz sinewave voice is sent to the sounder for broadcasting and simulating the surrounding disturbance. As shown in Fig. 7, the phase signals for the both branches are extracted simultaneously. For the 22 km sensing path, Fig. 7(a) shows the demodulated phase signal at the vibration position in time domain. Quasi-sinusoidal signal is recovered corresponding to the driving signal to the PZT. The undulating appearance may be due to low SNR with unwanted nonlinear effect induced. Similarly, Fig. 7(b) shows the demodulated phase signal for the 1 km sensing path. The fibre disturbance caused by the sounder is depicted through this phase information. Perfect sinusoidal

shape is recovered for this branch, which indicates that this branch can be used for sound tracking. In general, it can be seen that two sinusoidal curves with 100 Hz and 1 kHz frequencies are obtained, indicating successful measurement of fibre vibration for the both branches.
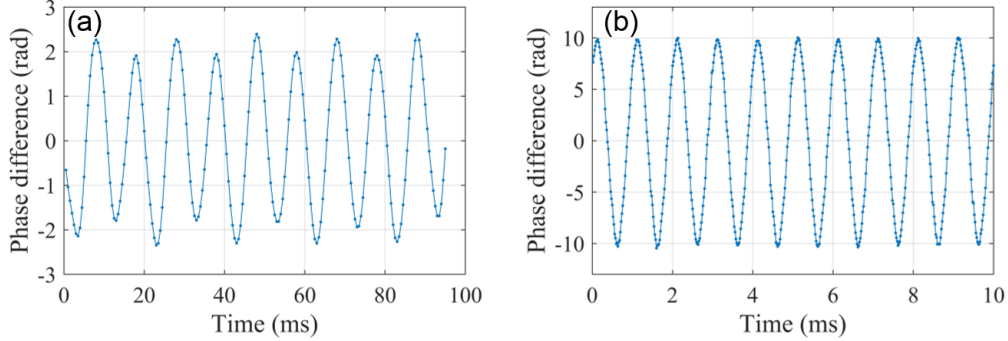

Fig. 7. The measurement results of phase demodulation in the time domain at the vibration location for (a) the 22 km fibre and (b) the 1 km fibre.
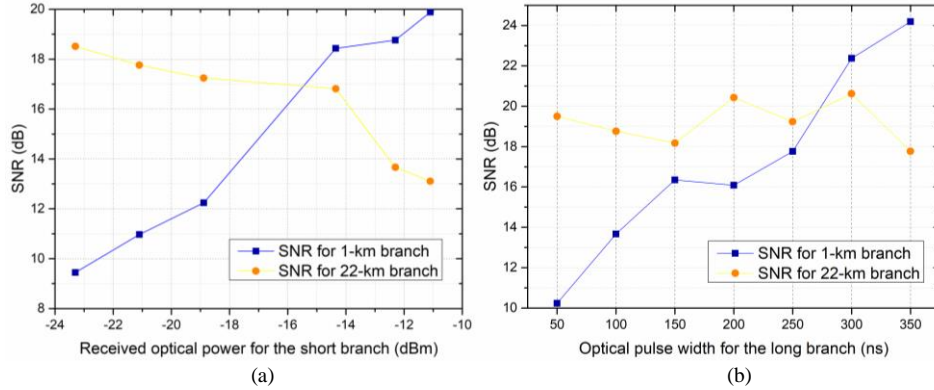

Fig. 8. The measured SNRs for the two branches (a) as the received optical power for the 1 km branch increases; and (b) as the optical pulse width for the 22 km branch increases.

To study the interference effect between the two branches, two experiments are further arranged. In the first experiment, we change the received optical power for the 1 km sensing fibre by adjusting the output of EDFA4, and keep the other branch's power unchanged. Then the averaged SNRs for the both branches are measured. Fig. 8(a) shows the results as the received power for the 1 km sensing fibre increasing from -23.3 dBm to -11.1 dBm. Due to this power increase, the SNR for this branch increases from 9.44 dB to 19.88 dB. But the SNR for the other branch with 22 km sensing fibre decreases from 18.51 dB to 13.11 dB due to the interference. Thus, to get an optimized SNR for every branch, a trade-off should be made for the optical power of every branch. In the second experiment, we change the optical pulse width for the 22 km sensing path from 50 ns to 350 ns, and keep the other branch unchanged. Fig. 8(b) shows the measured SNRs for the both branches in this situation. We can see that as the pulse width for the 22 km sensing path increases, the SNR for this branch drastically increases from 10.24 dB to 24.19 dB, and the SNR for the other branch seems to be maintained in the same level. In a practical MP-DAS system, it may be required to increase the SNR for the long sensing path. One method is to amplify the optical power of this branch, but this will bring interference and decrease the SNRs for the other branches. Another possible method is to increase the pulse width of this branch. This will not significantly decrease the SNRs for the other branches, however, the spatial resolution is sacrificed.

Further, we record a sound of hammer hitting and send it to the sounder to imitate the realistic scenario. The original sound shape and its corresponding short-time Fourier transform (STFT) are shown in Fig. 9(a1) and (b1). Fig. 9(a2) and (b2) show the information of the recovered phase signal for the separate measurement, and Fig. 9 (a3) and (b3) show that with two-path monitoring as discussed above. We can see that the retrieved phase signal is recovered successfully for both the two-path and separate monitoring situations. Due to the lower SNR for the two-path monitoring situation, we observe stronger noise in both time and frequency domain, as shown in Fig. 9(a3) and (3). Despite this, the audio can be easily recovered. All these three audio files (*i.e.*, one original hammer sound and two recovered audio files) are uploaded as the supplementary materials. The background noise is found for the recovered signals, but there is no big difference between the audios for separate monitoring and two-path monitoring situations. People can easily recognize the hammer sound, which indicates that our proposed MP-DAS works well for different application demands.
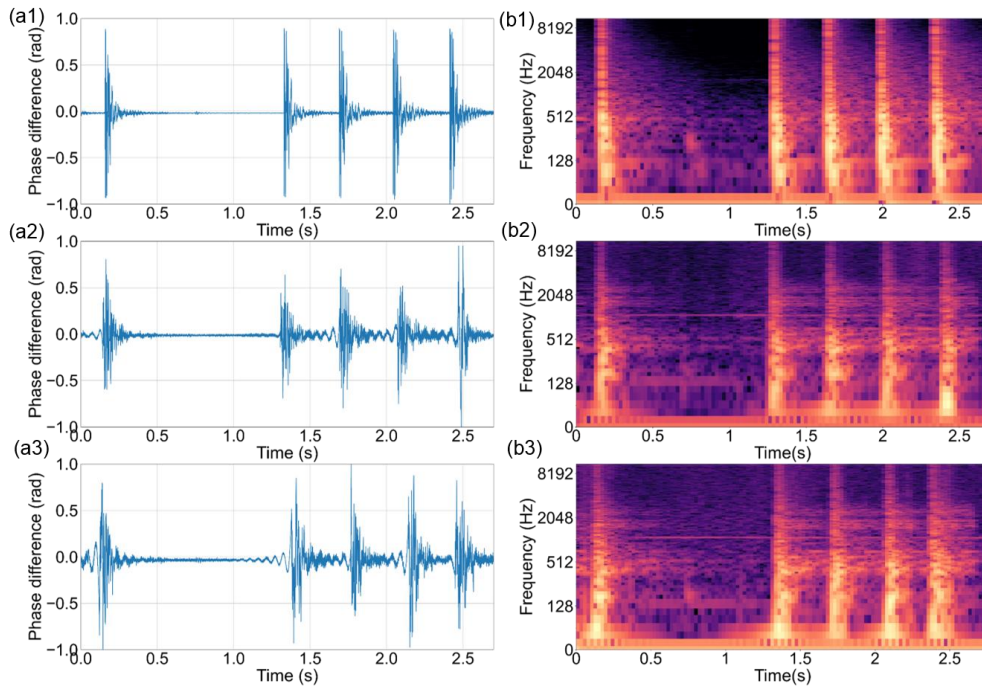

Fig. 9. The phase information of hammer hitting in time domain and its corresponding STFT, (a1), (b1) for the original hammer soundtrack; (a2), (b2) for the recovered signal with separate measurement; (a3), (b3) for the recovered signal with two-path monitoring.

4. Conclusion

In summary, we propose a MP-DAS system by introducing FDM technique to the Φ-OTDR with heterodyne detection. With the FDM technique, the single narrow-linewidth optical source and signal receiving end can be shared to all the sensing fibre paths with different requirements on the sensing distance, spatial resolution, frequency response, *etc*. It should be mentioned that for each sensing path, we still need the individual modulator and amplifiers, and to support this DAS network, we may need to increase the laser power, enlarge the BPD bandwidth, and upgrade the acquisition system. With the increase of monitoring paths, the overall cost may be reduced compared with using multiple single-channel DAS systems. In the experiment, a dual path Φ-OTDR system with 22 km and 1 km sensing distances is demonstrated. The amplitude and phase information of the two sensing paths are demodulated simultaneously for the

disturbance locating and dynamic vibration detection. To increase the SNR for a certain sensing path, a good approach is increasing the pulse width of this branch rather than directly amplifying its optical power. This mitigates the SNR's decrease for the other branches, but sacrifices the spatial resolution. We imitate different scenarios by using PZT vibration and sounder broadcasting, which shows our MP-DAS is suitable and subservient in the applications for multipath monitoring in complicated environment.

Acknowledgements

Declaration of competing interest

The authors declare that they have no known competing financial interests or personal relationships that could have appeared to influence the work reported in this paper.

References

1. Masoudi A, Newson TP. Contributed review: Distributed optical fibre dynamic strain sensing. Rev Sci Instrum 2016;87(1):011501.
2. Muanenda Y. Recent advances in distributed acoustic sensing based on phase-sensitive optical time domain reflectometry. J Sensors 2018;2018:1-16.
3. Guo H, Xiao G, Mrad N, Yao J. Fiber optic sensors for structural health monitoring of air platforms. Sensors 2011;11(4):3687-3705.
4. Tejedor J, Martins HF, Piote D, Macias-Guarasa J, Pastor-Graells J, Martin-Lopez S, Guillen PC, Smet FD, Postvoll W, Gonzalez-Herraez M. Toward prevention of pipeline integrity threats using a smart fiber-optic surveillance system. J Lightw Technol 2016;34(19):4445-4453.
5. Tejedor J, Macias-Guarasa J, Martins HF, Pastor-Graells J, Martin-Lopez S, Guillen PC, Pauw GD, Smet FD, Postvoll W, Ahlen CH, Gonzalez-Herraez M. Real field deployment of a smart fiber-optic surveillance system for pipeline integrity threat detection: Architectural issues and blind field test results. J Lightw Technol 2018;36(4):1052-1062.
6. Miah K, Potter DK. A review of hybrid fiber-optic distributed simultaneous vibration and temperature sensing technology and its geophysical applications. Sensors 2017;17(11):2511.
7. Schenato L. A review of distributed fibre optic sensors for geo-hydrological applications. Appl Sci 2017;7(9):896.
8. Peng F, Duan N, Rao Y, Li J. Real-time position and speed monitoring of trains using phase-sensitive OTDR. IEEE Photon Technol Lett 2014;26(20):2055-2057.
9. Wang Z, Lu B, Zheng H, Ye Q, Pan Z, Cai H, Qu R, Fang Z, Zhao H. Novel railway-subgrade vibration monitoring technology using phase-sensitive OTDR. Proc SPIE 2017;10323:103237G.
10. Wu Y, Gan J, Li Q, Zhang Z, Heng X, Yang Z. Distributed fiber voice sensor based on phase-sensitive optical time-domain reflectometry. IEEE Photon J 2015;7(6):6803810.
11. Lu Y, Zhu T, Chen L, Bao X. Distributed vibration sensor based on coherent detection of phase-OTDR. J Lightw Technol 2010;28(22):3243-3249.
12. Liokumovich LB, Ushakov NA, Kotov OI, Bisyarin MA, Hartog AH. Fundamentals of optical fiber sensing schemes based on coherent optical time domain reflectometry: Signal model under static fiber conditions. J Lightw Technol 2015;33(17):3660-3671.
13. Masoudi A, Newson TP. Analysis of distributed optical fibre acoustic sensors through numerical modelling. Opt Express 2017;25(25):32021-32040.
14. Liu H, Pang F, Lv L, Mei X, Song Y, Chen J, Wang T. True phase measurement of distributed vibration sensors based on heterodyne φ-OTDR. IEEE Photon J 2018;10(1):7101309.
15. Wang Y, Jin B, Wang Y, Wang D, Liu X, Bai Q. Real-time distributed vibration monitoring system using Φ-OTDR. IEEE Sensors J 2017;17(5):1333-1341.
16. He X, Xie S, Liu F, Cao S, Gu L, Zheng X, Zhang M. Multi-event waveform-retrieved distributed optical fiber acoustic sensor using dual-pulse heterodyne phase-sensitive OTDR. Opt Lett 2017;42(3):442–445.
17. Masoudi A, Belal M, Newson TP. A distributed optical fibre dynamic strain sensor based on phase-OTDR. Meas Sci Technol 2013;24(8):085204.

18. Masoudi A, Newson TP. High spatial resolution distributed optical fiber dynamic strain sensor with enhanced frequency and strain resolution. Opt Lett 2017;42(2):290-293.
19. Fang G, Xu T, Feng S, Li F. Phase-sensitive optical time domain reflectometer based on phase-generated carrier algorithm. J Lightw Technol 2015;33(13):2811-2816.
20. Fan X, Yang G, Wang S, Liu Q, He Z. Distributed fiber-optic vibration sensing based on phase extraction from optical reflectometry. J Lightw Technol 2017;35(16):3281-3288.
21. Xue N, Fu Y, Lu C, Xiong J, Yang L, Wang Z. Characterization and compensation of phase offset in Φ-OTDR with heterodyne detection. J Lightw Technol 2018;36(23):5481-5487.
22. He H, Shao L, Li Z, Zhang Z, Zou X, Luo B, Pan W, Yan L. Self-mixing demodulation for coherent phase-sensitive OTDR system. Sensors 2016;16(5):681.
23. Wang Z, Zhang L, Wang S, Xue N, Peng F, Fan M, Sun W, Qian X, Rao J, Rao Y. Coherent Φ-OTDR based on I/Q demodulation and homodyne detection. Opt Express 2016;26(2):853-858.
24. Armstrong J. OFDM for optical communications. J Lightw Technol 2009;27(3):189-204.
25. Zhou J, Pan Z, Ye Q, Cai H, Qu R, Fang Z. Characteristics and explanations of interference fading of a ϕ-OTDR with a multi-frequency source. J Lightw Technol 2013;31(7):2947-2954.
26. Iida H, Toge K, Ito F. Pulse waveform manipulation in FDM-OTDR for suppressing inter-channel crosstalk. J Lightw Technol 2014;32(14):2569-2576.
27. Yang G, Fan X, Liu Q, He Z. Frequency response enhancement of direct-detection phase-sensitive OTDR by using frequency division multiplexing. J Lightw Technol 2018;36(4):1197-1203.
28. He Q, Zhu T, Zhou J, Diao D, Bao X. Frequency response enhancement by periodical nonuniform sampling in distributed sensing. IEEE Photon Technol Lett 2015;27(20):2158-2161.
29. Wang Z, Pan Z, Fang Z, Ye Q, Lu B, Cai H, Qu R. Ultra-broadband phase-sensitive optical time-domain reflectometry with a temporally sequenced multi-frequency source. Opt Lett 2015;40(22):5192-5195.
30. Iida D, Toge K, Manabe T. Distributed measurement of acoustic vibration location with frequency multiplexed phase-OTDR. Opt Fiber Technol 2017;36:19-25.
31. Lu B, Pan Z, Wang Z, Zheng H, Ye Q, Qu R, Cai H. High spatial resolution phase-sensitive optical time domain reflectometer with a frequency-swept pulse. Opt Lett 2017;42(3):391-394.
32. Zou W, Yang S, Long X, Chen J. Optical pulse compression reflectometry: proposal and proof-of-concept experiment. Opt Express 2015;23(1):512-522.
33. Wu Y, Wang Z, Xiong J, Jiang J, Lin S, Chen Y. Interference fading elimination with single rectangular pulse in Φ-OTDR. J Lightw Technol 2019;37(13):3381-3387.
34. Wu Y, Wang Z, Xiong J, Jiang J, Rao Y. Bipolar-coding Φ-OTDR with interference fading elimination and frequency drift compensation. J Lightw Technol 2019;38(21):6121-6128.
35. Jiang J, Wang Z, Wang Z, Wu Y, Lin S, Xiong J, Chen Y, Rao Y. Coherent Kramers-Kronig receiver for Φ-OTDR. J Lightw Technol 2019;37(18):4799-4807.